Flexural deformations of URM piers: Comparison of analytical models with experiments

PETRY, SARAH[1]; BEYER, KATRIN[2];

ABSTRACT: Despite the fact that displacement-based methods are now frequently applied when assessing the seismic performance of unreinforced masonry (URM) structures, the displacement capacity of in-plane loaded URM piers is still estimated from empirical rather than mechanical relationships. One idea for estimating a pier's force-displacement curve including its displacement capacity that has been put forward in the past is based on the double integration of the curvature profile. The curvature is derived assuming a bilinear stress-strain relationship in the compression domain and neglecting the tensile strength of the masonry.

We tested several identical URM piers under different constant axial load and shear span ratios while applying quasi-static horizontal cyclic in-plane loading. During testing, we tracked with a set of cameras the displacement of four LEDs on each full brick of the masonry piers. Therefore, we were able to determine the local deformations, e.g. average strains in the bricks and deformations of the joints. In this paper we will present experimentally determined local and global deformation quantities of one pier dominated by flexural deformations and compare these to the estimates from the analytical model. Differences between model and experiment will be discussed and first estimates of performance limits describing local deformations will be proposed.

Keywords: Rocking, URM piers, Displacement based design, Flexural deformation

NOTATION

A Section of the pier;
C *Reduction factor for an equivalent rectangular stress bloc;*
E Modulus of elasticity perpendicular to the bottom joint;
f_u Compression strength perpendicular to the bottom joint;
G Shear modulus of elasticity of the masonry parallel to the bottom joint;
H Height of the pier;
H_0 Shear span;
h_c Height over which bed joint opening develops;
h_p Height of the plastic zone;
I Moment of inertia;
L Length of the pier;
L_c Length of compressed zone;
$L_{c,y}$ Length of compressed zone when the maximum admissible stress is reached;
$L_{c,u}$ Length of compressed zone at ultimate stage;
M Bottom moment;

[1)] Sarah Petry, Earthquake Engineering and Structural Dynamics (EESD), School of Architectural, Civil and Environmental Engineering (ENAC), École Polytechnique Fédérale de Lausanne (EPFL), sarah.petry@epfl.ch
[2)] Katrin Beyer, Earthquake Engineering and Structural Dynamics (EESD), School of Architectural, Civil and Environmental Engineering (ENAC), École Polytechnique Fédérale de Lausanne (EPFL), katrin.beyer@epfl.ch

M_e Bottom moment when bottom joint starts opening;
M_y Bottom moment when minimum admissible stress is reached;
M_u Bottom moment at ultimate point;
N Normal force applied to the pier;
T Width of the pier;
u Top displacement;
u_e Top displacement when bottom joint starts opening;
u_{fl} Top displacement caused by flexural deformations;
u_{sh} Top displacement caused by shear deformations;
V Lateral shear force;
V_e Lateral shear force when bottom joint starts opening;
α Shear span ratio;
Δ_p Plastic displacement;
ε_c Ultimate compression strain;
θ Rotation of the pier at top of the plastic zone;
θ_p Plastic rotation;
μ Coefficient considering the normal force shear force interaction on the displacement;
η Coefficient considering the normal force shear force interaction on the displacement;
ψ Displacement of the pier at top of the plastic zone;
X Curvature in bottom section;
X_y Curvature in bottom section when minimum admissible stress is reached;
X_u Curvature in bottom section at ultimate point;

1 INTRODUCTION

Despite the fact that displacement-based methods are now frequently applied when assessing the seismic performance of unreinforced masonry (URM) structures, the displacement capacity of in-plane loaded URM piers is still estimated from empirical rather than mechanical relationships. Already some decades ago first models were developed which describe the force-displacement relationship of unreinforced masonry (URM) structures that are mainly subjected to flexural deformations. Some of these models are of analytical nature and derive a direct relationship between horizontal force and top displacement; examples are the force-displacement relationship for leaning towers [1] or the force-displacement relationship developed in [2]. Others obtain the force-displacement relationship with the help of computer software based on macro-elements, for instance the model used in [3]. All these models have in common that they assume a no-tension material with a linear-elastic behaviour in compression. Hence, for small lateral loads the pier behaves linear-elastically until the maximum stress in the bottom section is equal to zero and the base section starts opening (see Figure 1, $V \leq V_e$). In the following, the effective section reduces and the flexibility of the pier increases. However, for small bottom joint openings, the URM pier remains undamaged and the residual displacement after unloading is negligible. Hence, the deformations are reversible and thus, until the onset of crushing at the toe, the pier's behaviour is almost non-linear elastic.

Ongoing from the basic assumption of a no-tension material and the linear-elastic and non-linear domain, Benedetti and Steli [2] developed analytically a model which relates the top displacement directly to the shear force of a URM pier. The model is developed for piers subjected to a constant normal force without rotational restraint at the top, hence, for piers tested under cantilever conditions. For piers subjected to fixed-fixed boundary conditions, Benedetti and Steli [2] propose calculating the displacement at half height of the pier and then, to double this displacement in order to obtain the displacement at the top of the pier. However, in [4] we show that in real structures, the boundary conditions which apply to a pier diverge from a cantilever or fixed-fixed boundary conditions. In order to extend the applicability of the model proposed by Benedetti and Steli [2], we review the basic ideas and extend the model for piers tested with variable boundary conditions. Furthermore, we compare the performance limits as described in [2] with the model developed by Priestley et al. [5] and compare the estimates with the experimental results we obtained from own tests [4].

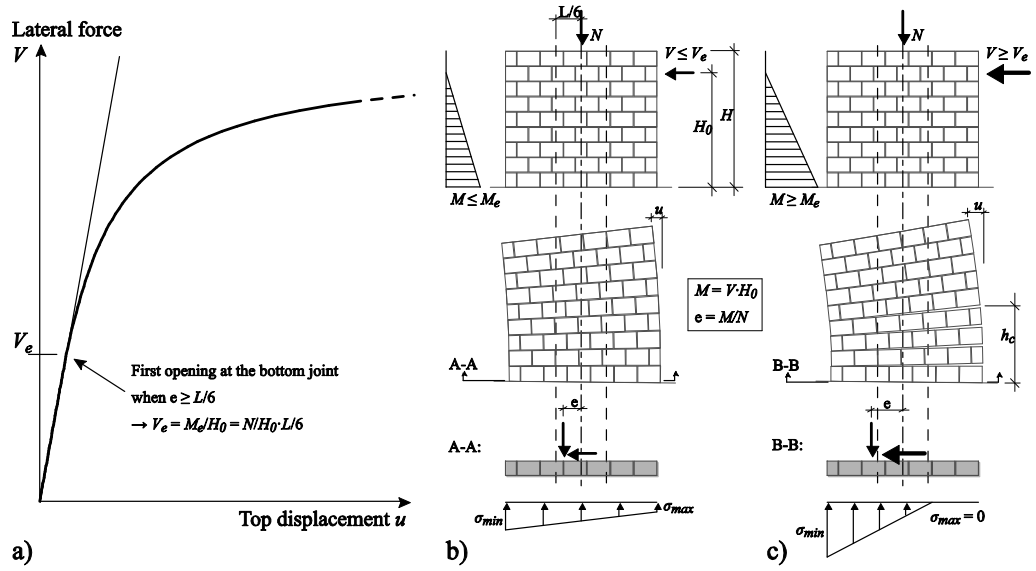

Figure 1. Force-displacement relationship for a no-tension material with linear-elastic behaviour in compression

2 MODELS FOR THE FORCE-DISPLACEMENT RELATIONSHIP OF MASONRY PIERS

2.1. Analytical model for the elastic shear force-displacement relationship of URM piers under cantilever conditions

The elastic domain of the model described by Benedetti and Steli [2] can be divided into two parts: First, the linear-elastic domain without opening of the bottom joint and second, the non-linear elastic domain with opening of the bottom joint. In the first domain ($V \le V_e$) the displacement u at the top of the pier is given as follows [2]:

$$u = V \cdot \frac{H^3}{3EI} + V \cdot \frac{H}{1.2\,GA} \qquad (1)$$

The first term of Eq. (1) accounts for the flexural deformations and the second part accounts for the shear deformation. E and G are the elastic and shear modulus of the masonry and $I = L^3T/12$ and $A = LT$ the geometrical properties of the section (L, T and H are the length, width and height of the pier).

When the moment in the bottom section ($M = VH_0$) exceeds the linear-elastic limit moment ($M_e = NL/6$), the bottom joint starts opening up, see Figure 1, and the curvature becomes [2]:

$$\chi = \frac{2N}{E \cdot T \cdot L_c^2} \qquad (2)$$

where L_c is the length of the compressed zone. In [2], the force-displacement relationship is obtained through linear interpolation of the linear and non-linear part:

$$u = u_e \cdot \frac{V_e}{V} + \theta(V) \cdot \frac{M_e}{V} + \psi(V) \qquad (3)$$

where u_e is the linear-elastic displacement for $V = V_e$. $\theta(V)$ and $\psi(V)$ are the rotation and displacement at top of the cracked zone (h_c, see Figure 1). They are given as follows [2]:

$$\theta(V) = -\frac{2N^2}{9ETLV}(2\mu - 12\eta) \tag{4}$$

$$\psi(V) = -\frac{N^3}{9ETV^2}\left(\mu - 6\eta + 2\ln\left(\frac{2\mu}{3}\right)\right) \tag{5}$$

$$\mu = \frac{L \cdot N}{L \cdot N - 2H \cdot V} \tag{6}$$

$$\eta = \frac{H \cdot V}{L \cdot N - 2H \cdot V} \tag{7}$$

Note that in Eq. (3) Benedetti and Steli [2] reduce the elastic displacement u_e from Eq. (1) in order to account for the reduced section at the bottom of the pier. However, they do not differentiate between flexural and shear deformations. While an increase of flexural flexibility due to cracking is considered by the second and third term of Eq. (3), this is not the case for the shear deformations. Eq. (3) assumes thus a decrease of the shear flexibility with crack propagation. To the authors' understanding this is not correct and Section 3.1 proposes therefore a revised formulation which treats flexural and shear deformations separately and which corrects further the flaws of the formulation in [2] (i.e. errors in Eqs. (3) to (5)).

2.2. Models for estimating the displacement capacity

The model by Benedetti and Steli [2] relates the local deformation of the compressed zone to the global displacement of the pier. However, in order to use the model for estimating the pier's displacement capacity, global displacement capacities have to be associated to deformation limits at the local level. To the authors' knowledge, two approaches are reported in the literature, which allow doing so: first, the so-called "yield" and "ultimate point" described by Benedetti and Steli [2] and second, the displacement capacity for flexural rocking given in Priestley et al. [5].

Benedetti and Steli [2] compute the displacement capacity by means of the yield and ultimate point. The yield point is determined as the point of the non-linear elastic domain (see previous section) when the minimum stress in the base section (see Figure 1) reaches the compression strength $\sigma_{min} = -f_u$ of the masonry. Hence, the so-called yield moment M_y is obtained as follows:

$$M_y = N\left(\frac{L}{2} - \frac{L_{c,y}}{3}\right) = \frac{L \cdot N}{2} - \frac{2N^2}{3T \cdot f_u} \tag{8}$$

$L_{c,y}$ represents the length of the compression zone at the yield point. Once the moment in the bottom section exceeds the yield moment, Benedetti and Steli [2] assume an elastic-ideal plastic material behaviour and therefore allow for a limited stress redistribution in the compressed zone. They proposed the following formula for computing the length of the compression zone $L_{c,u}$ and the admissible moment M_u at ultimate point [2]:

$$L_{c,u} = \frac{1.5 \cdot N}{T \cdot f_u} \tag{9}$$

$$M_u = N \cdot \left(\frac{L}{2} - 0.361 L_{c,u}\right) \tag{10}$$

In order to obtain an estimate for the remaining displacement capacity in the non-elastic range ($M_y \leq M \leq M_u$) the plastic length h_p is computed to be equal to the height of the pier subjected to higher moments than the yield moment [2]:

$$h_p(V) = H \cdot \left(1 - \frac{M_y}{M_u}\right) \tag{11}$$

while the curvature at ultimate point is estimated as follows [2]:

$$\chi_u = \frac{\grave{o}_c}{L_{c,u}} \tag{12}$$

ε_c is the maximum admissible compression strain at the external fibre of the masonry. Accordingly, the maximum plastic displacement is:

$$\Delta_p = \frac{1}{2}\left(\chi_u - \chi_y\right) \cdot h_p \cdot \left(H - h_p\right) \tag{13}$$

and the total displacement at ultimate point can be obtained by adding the plastic displacement from Eq. (13) to the elastic displacement obtained with Eq. (3) [2].

Another similar mechanical model which estimates the displacement at ultimate point is proposed by Priestley et al. [5]. Unlike the previously presented model, they assume the plastic hinge length to be equal to the remaining uncompressed length of the bottom section ($h_p = L - L_{c,u}$) and estimate thus the plastic rotation at the base of the pier as follows:

$$\theta_p = \frac{\grave{o}_c}{L_{c,u}} \cdot \frac{L - L_{c,u}}{2} \tag{14}$$

This approach is based on the assumption of an equivalent rectangular stress bloc (C = 0.85). Hence, the maximum moment and the compressed length at ultimate point are [5, 6]:

$$M_u = N \cdot \left(\frac{L - C \cdot L_{c,u}}{2}\right) \tag{15}$$

$$L_{c,u} = \frac{N}{C^2 \cdot f_u \cdot T} \tag{16}$$

Priestley et al. [5] refer later to the base rotation as the interstorey drift at the ultimate stage. Hence, we assume that the top displacement at ultimate point can be calculated as follows:

$$u_u = \theta_p \cdot H = \frac{\grave{o}_c}{L_{c,u}} \cdot \frac{L - L_{c,u}}{2} \cdot H \tag{17}$$

3 EXTENDED ELASTIC FORCE-DISPLACEMENT RELATIONSHIP FOR MASONRY PIERS SUBJECTED TO DIFFERENT BOUNDARY CONDITIONS

The model presented in [2] was developed for piers loaded as simple cantilever piers. However, in order to apply the analytical model proposed by Benedetti and Steli [2] also to a pier which we tested with a shear span of H_0 = 1.5H, the model is extended in the next section for a variable shear span ratio $\alpha = H_0/H \geq 1.0$. For piers with a shear span ratio $0.5 \leq \alpha < 1.0$ the different limit stages have to be considered at the bottom and top of the pier. Hence, we propose a separate approach in Section 3.2 to deal with these piers. As noted previously, the shear deformations will be treated separately from the flexural deformations, since they will be affected differently by the geometrical nonlinearity when the bottom joint starts opening. At any point of loading, the total deformations can be computed as the sum of the flexural and the shear deformations.

3.1. Displacement due to flexural deformations

Through double integration of the curvature we obtain the following relationship for the force-displacement relationship:

$$u_{fl} = V \cdot \frac{H^3}{2EI}\left(\alpha - \frac{1}{3}\right) \quad \text{for } V \le V_e \tag{18}$$

$$u_{fl} = u_{e,fl} \cdot \left(\left(1 - \frac{\alpha^2(3-\alpha)}{3\alpha - 1}\right) \cdot \frac{V}{V_e} + \frac{3\alpha^2(1-\alpha)}{3\alpha - 1} \cdot \frac{V_e}{V} + \frac{2\alpha^3}{3\alpha - 1} \cdot \left(\frac{V_e}{V}\right)^2\right) + \theta(V) \cdot \left(H(1-\alpha) + \frac{M_e}{V}\right) + \psi(V) \tag{19}$$

for $V \ge V_e$

with

$$\theta(V) = -\frac{2N^2}{9ETLV}(\mu - 6\eta) \tag{20}$$

$$\psi(V) = -\frac{N^3}{9ETV^2}\left(\frac{2}{3}\mu - 4\eta + 2\ln\left(\frac{2}{3}\mu\right)\right) \tag{21}$$

$$\mu = \frac{L \cdot N}{L \cdot N - 2\alpha H \cdot V} \tag{22}$$

$$\eta = \frac{\alpha H \cdot V}{L \cdot N - 2\alpha H \cdot V} \tag{23}$$

However, when we evaluate Eqs. (19) to (23) for a simple cantilever beam (α = 1) we obtain results that differ from the results reported by Benedetti and Steli [2] (Eqs. (3) to (7)):

$$u_{fl} = u_{e,fl} \cdot \left(\frac{V_e}{V}\right)^2 + \theta(V) \cdot \frac{M_e}{V} + \psi(V) \tag{24}$$

With

$$\theta(V) = -\frac{2N^2}{9ETLV}(\mu - 6\eta) \tag{25}$$

$$\psi(V) = -\frac{N^3}{9ETV^2}\left(\frac{2}{3}\mu - 4\eta + 2\ln\left(\frac{2}{3}\mu\right)\right) \tag{26}$$

$$\mu = \frac{L \cdot N}{L \cdot N - 2H \cdot V} \tag{27}$$

$$\eta = \frac{H \cdot V}{L \cdot N - 2H \cdot V} \tag{28}$$

The differences between our equations (Eqs. (24) to (28)) and the equations given in [2] (Eqs. (3) to (7)) for a cantilever pier, considering only the flexural deformations, are shown in Figure 2.

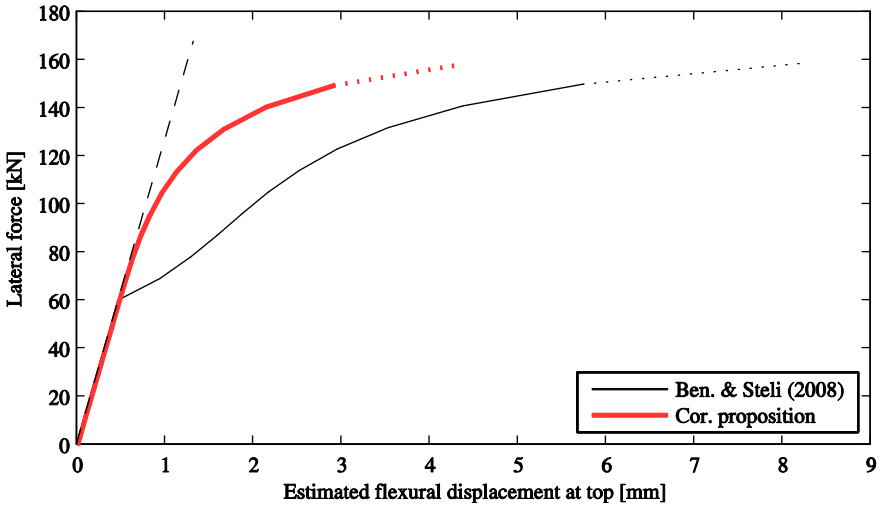

Figure 2. Force-flexural displacement relationship for a cantilever pier according to [2] and according to our corrected proposition

Even though both models are based on the same assumptions regarding the moment-curvature relationship, the resulting force-displacement relationships diverge at the onset of the non-linear elastic domain. The model in [2] predicts at the onset of the non-linearity an abrupt reduction of the flexibility, which is also shown in the graphs reported in [2]. The shape of the curve resembles that of a moment-curvature relationship of reinforced concrete but does not seem to be physically meaningful for URM. To verify our equations, we compared our model with the displacement obtained through numerical double integration of the curvature and obtained the same results for our analytical and numerical solution. This suggests that the equations in [2] include an error which was introduced in the integration process.

3.2. Displacement due to shear deformations

Since we consider a pier that is mainly subjected to flexural deformations, we assume that damage to the pier is only introduced through flexural deformations. Nevertheless, the shear deformations are not negligible. It is assumed that only the compressed section contributes to the shear stiffness. Hence, in analogy to the flexural deformations, the shear behaviour can be divided into the following same two domains: first, the linear domain while the whole section of the pier is in compression and the shear stiffness is independent of the flexural solicitation and second, the non-linear domain while the flexural deformations impose a crack opening in the bed joints and reduce thus the compressed area through which shear can be transferred.

In the linear-elastic domain ($V \leq V_e$) the shear deformations are independent of the moment profile of the pier. Hence, the shear displacement is as follows (see Eq. (3)):

$$u_{sh} = V \cdot \frac{5H}{6GA} \tag{29}$$

When the bottom joint starts opening, the effective area through which the shear stress is transferred reduces. Thus, the deformability increases and the following force-shear displacement relationship is obtained:

$$u_{sh} = u_{e,sh} \cdot \left(\alpha + \frac{V}{V_e}(1-\alpha) \right) + \psi_{sh}(V) \tag{30}$$

With

$$\psi_{sh}(V) = \frac{2N}{5GT} \cdot \ln\left(\frac{2}{3}\mu\right) \tag{31}$$

$$\mu = \frac{L \cdot N}{L \cdot N - 2\alpha H \cdot V} \tag{32}$$

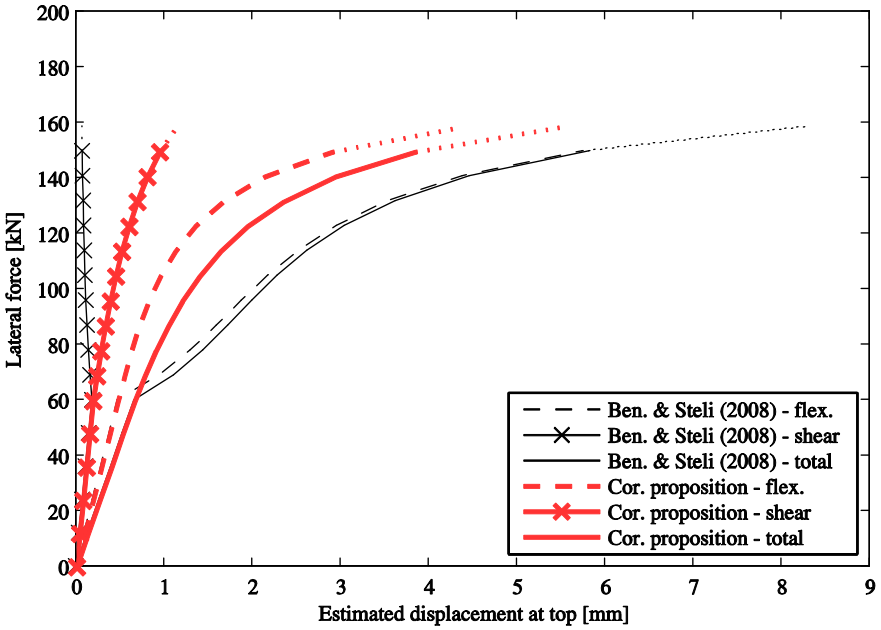

Figure 3. Force-displacement relationship for a cantilever pier according to [2] and according to our corrected proposition considering the different deformation components

From Figure 3 it can be noted that the model proposed in [2] predicts the shear deformation to decrease once bed joint opening takes place. As we mention previously, to the authors' opinion this is not realistic. In our model, the non-linear shear displacement is derived separately from the flexural displacement while considering the reduction of the effective section and it can be noted that we predict actually an increase in shear flexibility once the bottom joint starts opening.

3.3. Extension of the model for shear span ratios of $0.5 \leq \alpha = H_0/H \leq 1.0$

The model described in the previous section is also applicable for piers with a shear span lower than the pier height. For this, the authors propose the following procedure: First, the displacement $u_{1,0}$ at the inflection point can be computed using the equations presented in Sections 3.1 and 3.2 by replacing the pier height by the shear span and setting the shear span ratio to one, hence, $H^* = H_0$ and $\alpha^* = 1.0$. In a second step, the rotation at the inflection point $\theta_{1,0}$ can be computed using the following equations:

$$\theta(V) = \frac{V}{EI} H^2 \left(\alpha^* - \frac{1}{2}\right) \quad \text{for } V \leq V_e \tag{33}$$

$$\theta(V) = \frac{V}{EI} H^2 \left(\alpha^* - \frac{1}{2} - \frac{1}{2} \cdot \alpha^{*2} + \frac{1}{2} \cdot \left(\frac{V_e}{V}\right)^2\right) - \frac{2N^2}{9ETLV}(\mu - 6\eta) \quad \text{for } V \geq V_e \tag{34}$$

Then, the relative displacement developing between inflection point and top $u_{2,0}$ is obtained using again the equations presented in Sections 3.1 and 3.2 by replacing the pier height by the height

remaining above the inflection point and setting the shear span ratio again equal to one, hence, $H^* = H\text{-}H_0$ and $\alpha^* = 1.0$ (Note that the limit $V \leq/\geq V_e$ changes respectively to $V \leq/\geq H_0/(H\text{-}H_0)\ V_e$ for the part of the wall above the inflection point). As next step, the rotation $\theta_{2,0}$ is computed for the part of wall above the inflection point using again Eqs. (33) and (34). Finally, the displacement at top of the pier can be computed with the following equation:

$$u(V) = u_{1,0}(V) + u_{2,0}(V) + \left(\theta_{1,0}(V) - \theta_{2,0}(V)\right) \cdot (H - H_0) \qquad (35)$$

Note that the plastic displacement (see Section 2.2) should be added only once using the full height of the pier.

4 COMPARISON OF THE FORCE-DISPLACEMENT RELATIONSHIP WITH A PIER FAILING DUE TO FLEXURAL ROCKING

In order to evaluate the herein described models, the force-displacement relationship is compared to an URM pier which was tested under a cyclic quasi-static lateral force in in-plane direction in the structural laboratory of the EPF Lausanne, Switzerland. The experiment itself is presented elsewhere [4]. The dimensions of the pier were L x H x T = 2.01 x 2.25 x 0.20 m. The material properties which are used for the following discussion were taken from [4] and are summarized in Table 1. The test unit PUP3, which is chosen for comparison herein this article, was tested under a constant normal force of N = 419 kN (σ_0/f_u = 0.18) and with a constant shear span of H_0 = 1.5 H. Throughout the test, the deformation in the pier were dominated by a flexural behaviour. Even though shear cracks appeared just before reaching the peak strength, these did not develop further and did not cause any additional damage to the pier.

Table 1. Properties of the masonry

Masonry properties:			
Compression strength	f_u	5.87	MPa
E-modulus	E	3550	MPa
Poisson ratio	v	0.20	-
Shear modulus	$G = E/(2(1+ v))$	1479	MPa

In Figure 4, the force-top displacement of PUP3 is obtained from the average of the first loading envelopes in positive and negative loading direction. For comparison the displacement is estimated with our corrected model developed in Chapter 3, once without considering any stress limit and once using the stress limit $\sigma_{min} = -f_u$ [2] (= "yield point"). In addition, the ultimate displacement is estimated once adapting the criteria from [2] to our corrected model and once using the criteria from [5], (see Table 2). For both approaches an admissible compression strain of ε_c = 4 ‰ is assumed, e.g. [5].

In Figure 4, it can be noted that the curve obtained with our corrected proposition (see Chapter 3) matches perfectly with the force-displacement response obtained through experiments. However, this is not the case when we look at the predicted ultimate displacement. If we assume the ultimate displacement to be attained when the maximum force capacity drops by 20%, we can observe that for both approaches the ultimate displacement is underestimated. If we consider that the approaches base on similar basic ideas, for instance ε_c = 4 ‰, it is surprising that the estimates diverge so much from each other. This difference is mainly due to the choice of the plastic hinge length. In [5], it is assumed that the plastic zone propagates at an angle of 45° and therefore, the plastic hinge length is assumed to depend only on the section of the pier and the normal stress ratio. Even though the model given by Priestley et al. [5] seems to yield a better estimate (see Figure 4), to the authors' opinion the

assumption done for the plastic hinge length is too simplistic and we suggest determining the actual plastic hinge length using Eq. (8) as proposed by Benedetti and Steli [2].

Table 2. Comparison of the ultimate displacement predicted with [2] and [5]

	Benedetti and Steli [2]		**Priestley et al. [5]**	
Compression length $L_{c,u}$	Eq. (8)	0.535 m	Eq. (16)	0.494 m
Moment capacity M_u	Eq. (9)	340 kNm	Eq. (15)	333 kNm
Ultimate curvature X_u	Eq. (12)	0.0075 m^{-1}	ε_c / $L_{c,u}$	0.0081 m^{-1}
Plastic hinge height h_p	Eq. (11)	0.186 m	L - $L_{c,u}$	1.152 m
Plastic displacement Δ_p	Eq. (13)	0.99 mm	-	-
Ultimate displacement u_u	Eq. (19) + Δ_p	4.83 mm	Eq. (17)	13.8 mm

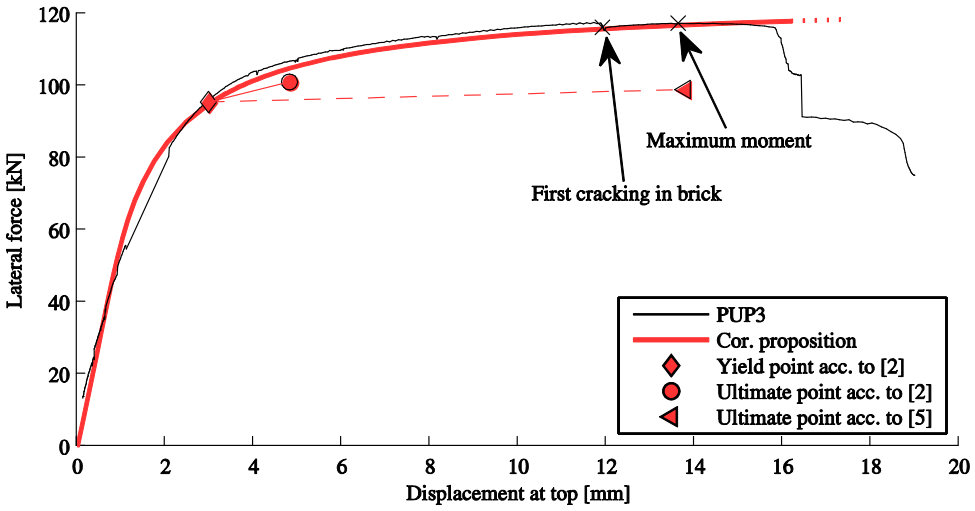

Figure 4. Corrected model with different approaches for estimating the displacement capacity versus the experimentally determined first-loading envelope of PUP3 H_0 = 1.5 H, N = 419 kN. “First cracking in brick” and “Maximum moment” relate to experimental observations.

Nevertheless, when adopting the limits by Benedetti and Steli [2] in our model, displacement and force capacity are underestimated. If we consider the yield point to be the point where non-reversible damage takes place, we can conclude that the yield point should coincide with the point where first cracks propagate through bricks. This idea is confirmed in Figure 4: when we extend our corrected model for stresses smaller than the compression strength, experiment and prediction match perfectly until the point where first cracking in brick occurs.

In Figure 5, the admissible compression stress was determined such that the yield point matches with first cracking in brick (→ $\sigma_{min} \approx -3.3 \cdot f_u$). It can be noted that using this limit stress leads also to a reasonable estimate for the ultimate displacement capacity when the lateral load of the pier drops to 80 % of the peak load.

Considering that vertical and shear stresses have to be transferred through the compressed zone, a biaxial stress state can be assumed in the compressed zone. Several researchers report the compression strength of masonry to increase when subjected to biaxial in-plane loading, e.g. [7].

Nevertheless, the admissible minimum stress which we determined to match yield point and first cracking in brick is significant lower than the compression strength ($|\sigma_{min}|/f_u \approx 3.3$). In comparison the ratios between compression strength and minimum admissible stress reported in [7] are significant smaller ($\sigma_{min}|/f_u << 2$). Therefore, we concluded that another phenomenon must take place which confines further the masonry and allows therefore for such low minimum stress.

However, from Figure 5 it can be noted that the choice of the minimum stress has relative little impact on the force capacity ($V_{y,exp} / V_{y,mod} \sim 1.2$), while it has a big impact on the displacement capacity ($u_{y,exp} / u_{y,mod} \sim 4$). The maximum moment is limited for small compression length ($L_c << L$), since the effective lever arm cannot increase significantly (M must be smaller than $NL/2$). On the other hand, the curvature which determines the flexibility of the pier is proportional to L_c^{-3}, hence increases significantly for small compression lengths. Therefore, underestimating the admissible stress in the compression zone is unreasonable conservative when regarding the displacement capacity. Note, that the assumption of the stress distribution – for instance, the assumption of a triangular stress distribution in elastic range [2] or the assumption of an equivalent rectangular stress field [5, 6] – is not decisive for the minimum compression length and the moment capacity once $L_c << L$.

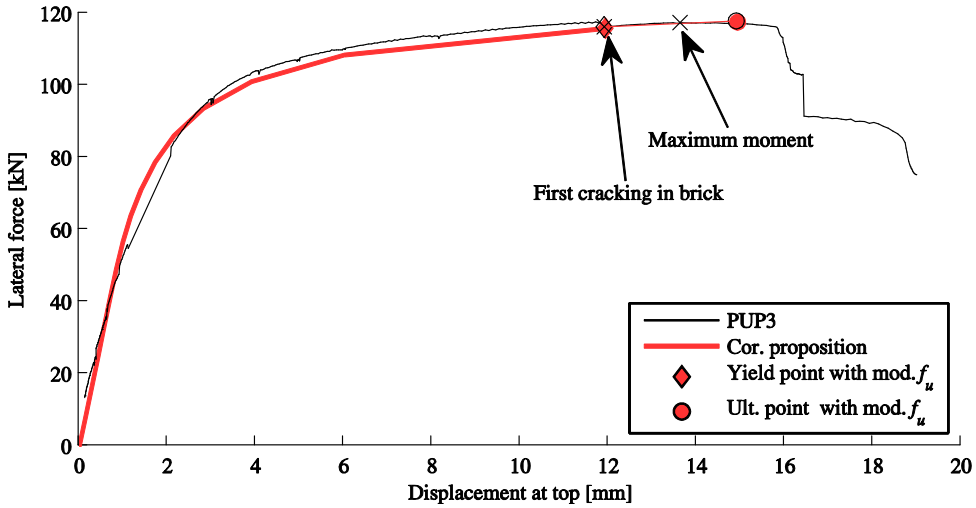

Figure 5. Corrected proposition while assuming an increased stress capacity versus first-loading envelopes of PUP3 $H_0 = 1.5\ H$, $N = 419$ kN

5 CONCLUSION

In this article we review first the existing model by Benedetti and Steli [2]. We discuss the model regarding the assumptions for shear and flexural deformations, we extend its validity to shear span ratios different to unity and correct the flaws in the equations in [2].

We then review two existing models which associate global displacement failure to local deformation limits (Benedetti and Steli [2]; Priestley et al. [5]) and compare the results to an experiment which we performed at the structural laboratory of the EPF Lausanne. The results showed that simplifying the determination of the plastic hinge height to the length of the non-compressed zone as proposed by Priestley et al. [5] can be too simplistic and we suggest using the approach given by Benedetti and Steli [2]. However, limiting the stress to the compression strength of masonry underestimates the strength and deformation capacity of the pier. While the choice of the minimum admissible stress has little impact on the force capacity, this is not the case for the displacement capacity. The choice of the admissible stress has a large influence on the compression length and thus on the deformability of the pier. Hence, we show that if the minimum stress is determined such that yield point and first cracking in brick coincide, we can actually predict the force-displacement relationship of URM piers dominated by a flexural behaviour.

We are currently working on the improvement of the local failure criteria in order to obtain a better estimate on the minimum admissible stress, such to match the prediction of the performance levels to local test observation. In addition, we are working on the validation against a larger set of tests and the development of a mechanical model for piers failing in shear.

REFERENCES

[1] Heyman, J.: Leaning towers. *Meccanica*, 27 (1992), 153-159.

[2] Benedetti, A. & Steli, E: Analytical models for shear-displacement curves of unreinforced and FRP reinforced masonry panels. *Construction and Buildings Materials*, 22 (2008) 175-185.

[3] Penna, A.; Lagomarsino, S. & Galasco, A. A nonlinear macroelement model for the seismic analysis of masonry buildings. *Earthquake Engineering and Structural Dynamics*, DOI: 10.1002/eqe.2335, 2013.

[4] Petry, S. & Beyer, K.: Influence of coupling on the displacement capacities of URM piers – comparison of experimental results with existing recommendations. In: *Proc. of the Vienna Congress on Recent Advances Earthquake Engineering and Structural Dynamics*, eds. S. Adam, R. Heuer, W. Lenhardt & C. Schranz, Vienna (2013), 1-10.

[5] Priestley, M.J.N.; Calvi, G.M. & Kowalsky, M.J.: *Direct Displacement Based Design*. IUSS PRESS, Pavia 2007.

[6] Magenes, G. & Calvi, G.M.: In-plane seismic response of brick masonry walls. *Earthquake Engineering and Structural Dynamics*, 26 (1997), 1091–1112.

[7] Lourenço, P.B.; Rots, J.G. & Blaauwendraad, J.: Continuum Model for Masonry: Parameter Estimation and Validation. *Journal of Structural Engineering*, 124 (1998), 642-652.